Received: 5 December 2017 | Revised: 23 August 2018 | Accepted: 5 September 2018

DOI: 10.4218/etrij.2017-0291

ORIGINAL ARTICLE

WILEY ETRI Journal

Ferrite-based wideband circularly polarized microstrip antenna design

Mostafa Mashhadi[1] | **Nader Komjani**[1] | **Behzad Rejaei**[2] | **Javad Ghalibafan**[3]

[1]Department of Electrical Engineering, Iran University of Science and Technology, Tehran, Iran

[2]Department of Electrical Engineering, Sharif University of Technology, Tehran, Iran

[3]Department of Electrical Engineering, Shahrood University of Technology, Shahrood, Iran

Correspondence
Nader Komjani, Department of Electrical Engineering, Iran University of Science and Technology, Tehran, Iran.
Email: n_komjani@iust.ac.ir

In this paper, a wideband, circularly polarized patch antenna is proposed that leverages the unidirectional resonant modes of a circular patch mounted on top of a grounded dielectric-ferrite substrate. The proposed antenna is fed via the proximity coupling method and several parasitically coupled patches are placed on a dielectric superstrate to enhance the impedance bandwidth of the antenna. The resonant modes of the structure rotate only in the clockwise or counter clockwise directions. In the frequency range where the effective permeability of the ferrite layer is negative, the resonance frequencies of these modes differ significantly, which produces a large axial ratio (AR) bandwidth. For the proposed antenna, the numerical results show the 10 dB impedance bandwidth to be around 44% and the 3 dB axial ratio bandwidth to be higher than 64%.

KEYWORDS
axial ratio, ferrite substrate, microstrip antenna, stacked configuration, wideband circular polarization

1 | INTRODUCTION

Circularly polarized antennas are widely used in various wireless systems, including wireless local area networks, radio frequency identification tags, the global positioning system (GPS), and the global navigation satellite system as they reduce the relative constraints on the orientation and multipath and provide better weather penetration than linearly polarized antennas. Some methods to achieve circular polarization (CP) include truncating the patch corners [1], cutting a diagonal slot in the patch [2], adding a tuning stub to the patch [3], using the triple proximity-fed method [4], and using the Koch curve as a boundary to the triangular patch [5]. While broadband circularly polarized antennas have been proposed based on parasitic strips [6], metasurface superstrates [7], slot arrays [8], patch arrays [9], and split-ring resonator (SRR)-inspired slot antennas [10], the reported axial ratios (AR) of these antennas are <25%.

In [11], researchers employed a quad-feed network and quadruple patch to obtain a CP bandwidth of 72%; however, the network used to feed the antennas was relatively complicated. The planar slot antennas with a microstrip coplanar waveguide (CPW) feed that were presented in references [12,13] achieved an AR bandwidth of about 40%. In this case, a wideband CP was obtained by applying perturbations to the rectangular slot [12] and exciting the even and odd modes of the CPW with a 90° phase difference [13]. In references [14,15], printed rectangular and triangular monopoles were shown to achieve an AR bandwidth of more than 50%. Here, circular polarization was obtained via an asymmetric antenna design. While the feed networks of the antennas presented in references [12–15] were simple, the radiation patterns were omnidirectional, the antenna gains were small, and the beamwidths of the circular polarization were insufficient in some frequency ranges. To enhance the gain of these antennas, the researchers in references [16,17] proposed employing a frequency selective surface (FSS) as a reflector; however, this necessitated an increase in antenna dimensions.

In other research, microstrip patch antennas on a normally magnetized ferrite substrate were found to radiate a CP pattern [18–20]; however, the corresponding AR bandwidths and beamwidths were quite narrow as the clockwise and counter clockwise resonant modes were close in frequency and the coupling between these two opposite modes degraded the AR figures. To overcome these problems, Ghalibafan et al. presented a wide-angle circularly polarized antenna [21] designed to operate in the frequency range where ferrite has a negative effective permeability. As only clockwise or counter clockwise modes exist in this frequency range, the result is a wide-angle, wideband AR. However, due to the high permittivity of ferrite, the proposed antenna had a narrow impedance bandwidth of <1%. To improve this, the authors in reference [22] proposed an antenna consisting of a metallized ferrite disk mounted on a grounded dielectric substrate and showed analytically in reference [22] that the clockwise and counter clockwise resonance frequencies of this antenna differed significantly over the negative effective permeability range of the ferrite. Finally, the parasitic patch technique described in reference [22] has been employed to achieve an impedance bandwidth of 15.5%, which is still much less than the antenna AR bandwidth (50%).

In this paper, a new structure is proposed to counter the problems in the designs presented in references [21,22]. As a first step, the proposed structure consists of a circular patch antenna mounted on a two-layer dielectric-ferrite substrate and excited by a proximity-coupled feed line. This approach results in a broadband AR when the resonance occurs in the negative permeability range. The structure also incorporates parasitic patches in a stacked configuration to enhance the impedance bandwidth of the antenna. When simulated, the impedance bandwidth had increased by 44% over previous methods.

2 | TWO-LAYER DIELECTRIC-FERRITE MICROSTRIP ANTENNA

The structure of a circular microstrip patch antenna on a grounded, two-layer dielectric-ferrite substrate is shown in Figure 1. As shown, the antenna is fed by a proximity coupled feed line placed between the ferrite and dielectric layers and the ferrite substrate is magnetized vertical to the ground plane along the z-axis by a DC biased magnetic field H_0. The ferrite layer consists of yttrium iron garnet with a relative permittivity (ε_f) of 15.3, saturation magnetization of 0.173 T, magnetic line width of 10 Oe, and thickness (h_f) of 1 mm. The dielectric layer is assumed to be RT/D 5880 with a relative permittivity (ε_d) of 2.2 and thickness (h_d) of 0.8 mm. According to Ghalibafan et al. [21], the permeability $\mu_\perp$ is defined as follows:

$$\mu_\perp = \mu - \frac{\mu_a^2}{\mu} = \frac{(\omega_H + \omega_M)^2 - \omega^2}{(\omega_H(\omega_H + \omega_M))^2 - \omega^2}, \quad (1)$$

and has a negative value in the following frequency range:

$$\sqrt{\omega_H(\omega_H + \omega_M)} < 2\pi f < \omega_H + \omega_M, \quad (2)$$

where μ and μ_a are the diagonal and off-diagonal elements of the permeability tensor of the ferrite, respectively. In addition, $\omega_H = \gamma_{H0}$ and $\omega_M = \gamma_{MS}$, where M_S is the saturation magnetization and γ is the gyromagnetic ratio of ferrite [21]. The simulations in this study assumed a magnetic bias field of H_0 = 15,000 A/m and a negative value for $\mu_\perp$ in the frequency range 1.68 GHz < f < 5.35 GHz. The antenna was designed to operate at a frequency of 4.3 GHz. The dimensions of the antenna were optimized based on the listed specifications, which resulted in a = 6.5 mm, W_f = 1 mm, L_f = 12.5 mm, and L = 30 mm. The impedance matching of the antenna was realized by appropriately selecting the dimensions of the feed line to accommodate the values of W_f and L_f. Note that the radius of the patch determines the resonant frequency of the antenna. An initial approximation for the radius of the patch can be obtained by replacing the ferrite layer with a dielectric with the same relative permittivity and then applying the models presented for computing the resonant frequency of a circular patch antenna with a composite substrate [23–25]. Alternatively, the patch radius can be approximated using the semi-analytical method presented in Mashhadi et al. [22].

The simulations in this study were conducted using the high frequency structure simulator (HFSS) developed by Ansoft. The simulated results for the return loss, AR, and gain of the proposed antenna are shown in Figure 2. The simulated −10 dB impedance bandwidth was 180 MHz (4.2%), which is five times higher than the bandwidth obtained in [21]. The higher bandwidth was the result of increasing the antenna height and decreasing the effective

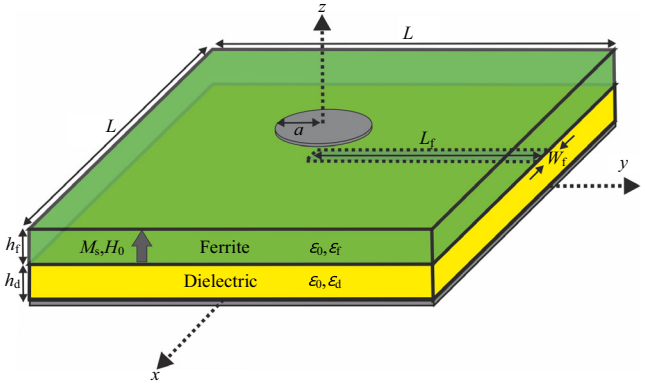

FIGURE 1 Schematic of two-layer dielectric-ferrite microstrip antenna excited with proximity-coupled feed line

permittivity of the structure by inserting a low permittivity dielectric layer between the ferrite and ground plane. The peak gain of the antenna was found to be 6 dB and the 3 dB AR bandwidth was more than 1.8 GHz, which is a direct consequence of the large separation in frequency between the clockwise and counter clockwise resonant modes, and was obtained by positioning the operating frequency in the negative $\mu_\perp$ range.

The clockwise resonant mode was dominant at the first resonance, as illustrated in Figure 3, where the current distribution on the patch at 4.3 GHz for four different time phases (ω_t) is plotted. Between 0° and 270° in intervals of 90°, the dominant surface current flowed in the directions of the y, x, $-y$, and $-x$ axes, respectively. In other words, as time passed, the surface current profile rotated in the clockwise direction, which resulted in a left-handed circular polarization (LHCP) in the $+z$ direction. The normalized circularly polarized radiation patterns of the antenna at 4.3 GHz on the x-z ($\varphi = 0°$) and y-z ($\varphi = 90°$) planes are presented in Figure 4. This antenna had an LHCP pattern with a front-to-back ratio (FBR) of 13 dB.

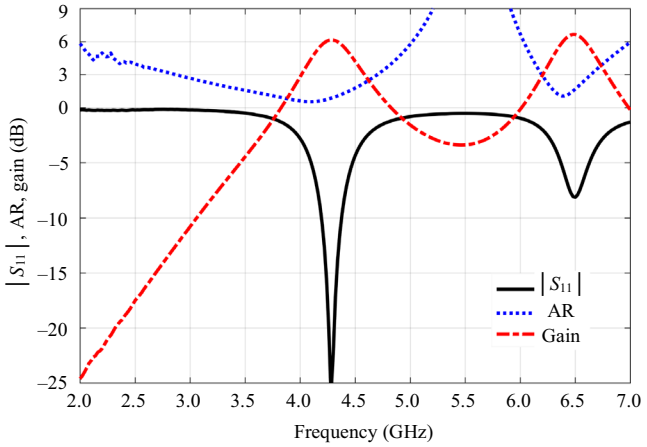

FIGURE 2 Full-wave simulation of $|S_{11}|$, axial ratio (AR), and gain for antenna shown in Figure 1

3 | PARASITICALLY COUPLED STACK CONFIGURATION

As described in the previous section, the antenna shown in Figure 1 had a wideband circular polarization; however, it also had a small impedance bandwidth. This can be addressed by employing impedance bandwidth enhancement techniques [26–30]. For example, the dual resonance method was used in references [27–30] to improve the impedance bandwidth of patch antennas.

Parasitic patches can be used in microstrip antennas for various purposes. For example, a U-shaped parasitic strip was used to realize a notch frequency band in [31], parasitic elements were used to achieve multi-band operation in

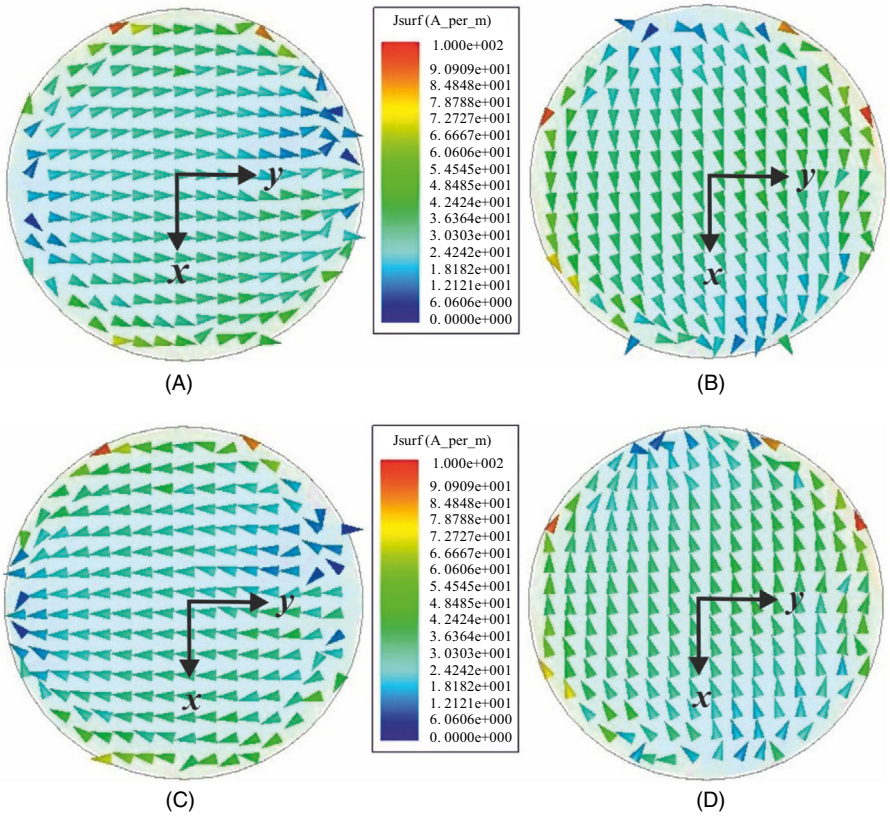

FIGURE 3 Surface current distributions on patch at 4.3 GHz for different time instants: (A) $\omega_t = 0°$, (B) $\omega_t = 90°$, (C) $\omega_t = 180°$, and (D) $\omega_t = 270°$

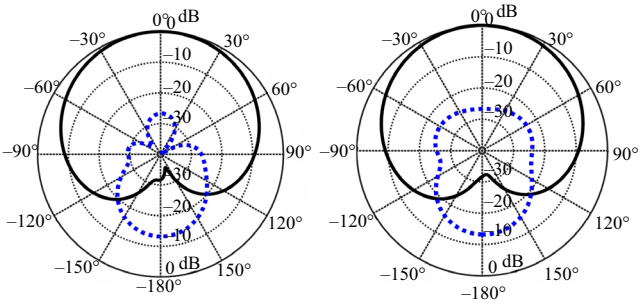

FIGURE 4 Normalized circularly polarized radiation patterns at $f = 4.3$ GHz (left-hand circularly polarized pattern: solid line, right-hand circularly polarized pattern: dotted line)

[32], the AR bandwidth of microstrip antennas was increased using parasitic patches in references [6,33], and parasitic patches were used to improve the impedance bandwidth of microstrip antennas in references [26]. In the latter case, one or several parasitic patches that had a resonance frequency close to the resonant frequency of the feed patch were placed close to the feed patch.

In the proposed design, a stacked configuration with multiple resonators is employed to increase the impedance bandwidth; however, instead of using the planar-coupled technique, two or more patches on different layers of the dielectric substrates are stacked on top of each other [26]. To further enhance the impedance bandwidth, these two techniques, namely, parasitic and stacked configurations, can be combined. The structure in Figure 5 combines both techniques to improve the impedance bandwidth of the original design.

The proposed antenna is composed of a two-layer microstrip patch antenna (similar to Figure 1) and four parasitic patches mounted on the upper side of a superstrate layer. The bottom patch is fed with a proximity-coupled feed line while the top parasitic patches are excited by electromagnetic coupling with the bottom patch. The superstrate is RO3010 with a relative permittivity (ε_s) of 10.2 and thickness (h_s) of 0.8 mm. The optimized antenna parameters are $b = 5.8$ mm, $S = 10$ mm, $g = 4.2$ mm, $W_f = 0.9$ mm, $L_f = 33$ mm, and $L = 50$ mm, while the other parameters are unchanged compared to the previous example. Because the resonance frequency of the parasitic patches was designed to be close to the resonant frequency of the feed patch, the initial approximation for the radius of the parasitic patches was assumed to be equal to the radius of the feed patch. Then, an accurate value of b was obtained by optimizing the radius of the parasitic patches using a full-wave simulation.

The antenna return loss, which was obtained via full wave simulations, is shown in Figure 6. The simulations were performed using two different software packages, namely, HFSS and the CST Microwave Studio (CST).

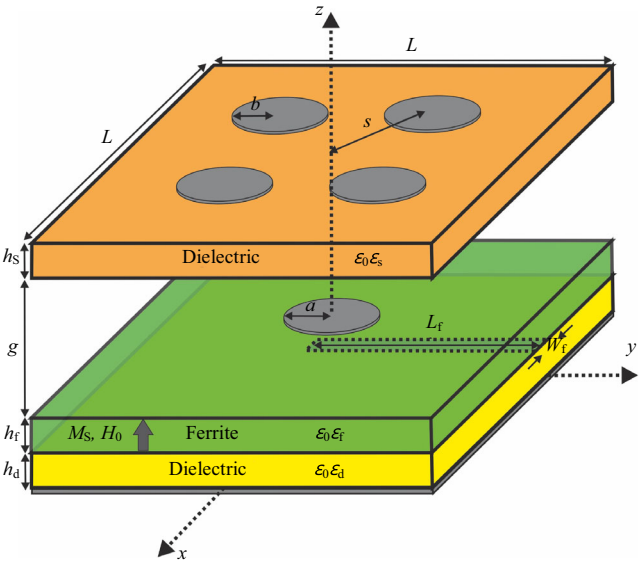

FIGURE 5 Proposed two-layer microstrip antenna with parasitic patches in stacked configuration

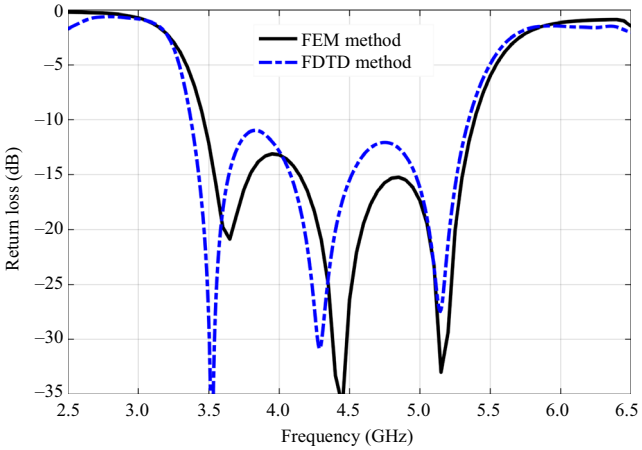

FIGURE 6 Comparison of two numerically independent methods for computing return loss of proposed antenna

The HFSS simulation was conducted in the frequency domain using the finite element method (FEM) while the CST simulation was performed in the time domain and was based on the finite difference time domain (FDTD) technique. The return losses obtained from the two methods exhibited good agreement and the impedance bandwidth of the proposed antenna was found to be more than 1.9 GHz (44%). The obtained impedance bandwidth was 10.5 times higher than that of the antenna shown in Figure 1, 54 times higher than the antenna described in Ghalibafan et al. [21], and almost three times higher than the antenna in Mashhadi et al. [22]. As shown in Figure 6, there are three in-band poles in the return loss response of antenna, two of which were produced by the main and parasitic patches.

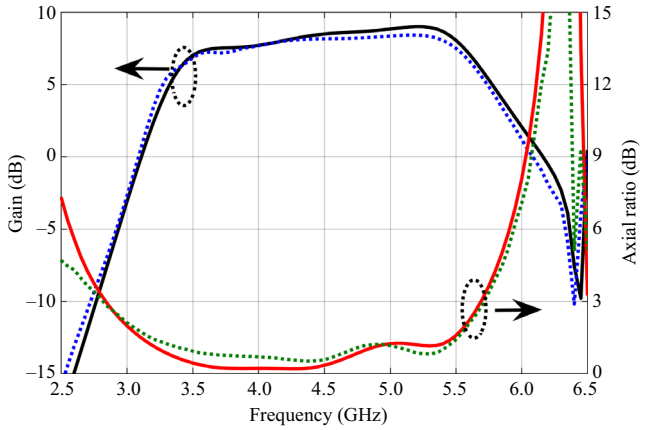

FIGURE 7 Comparison of gain and AR of proposed antenna, which were obtained via two numerically independent methods (solid line represents FEM method and dotted line represents FDTD method)

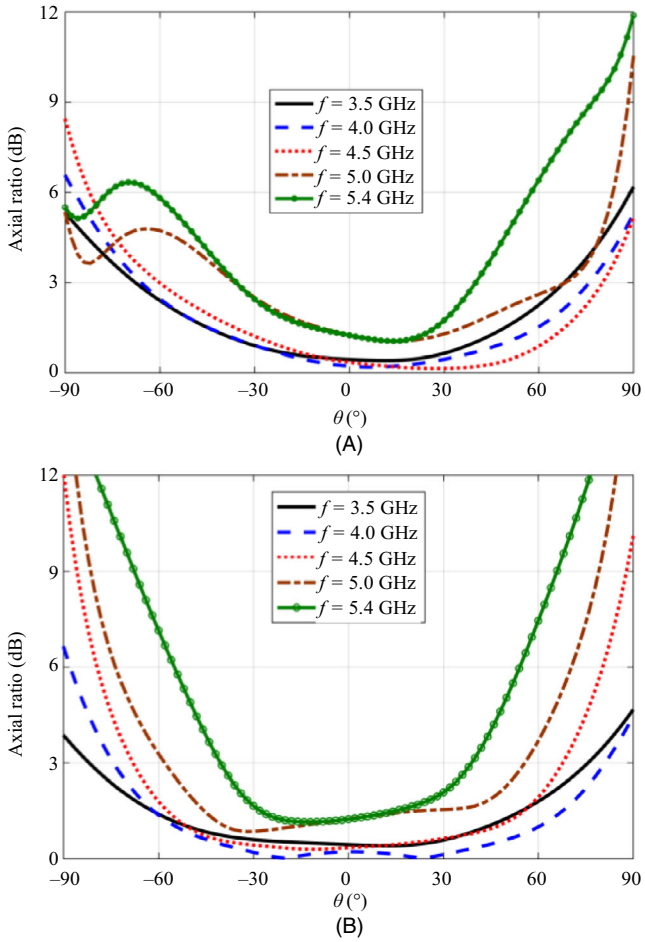

FIGURE 8 Antenna AR patterns at different frequencies: (A) *x*-*z* plane, and (B) *y*-*z* plane

Although not shown here for brevity, it can be easily shown via parameter sweeps that the third pole was created by the proximity feed line.

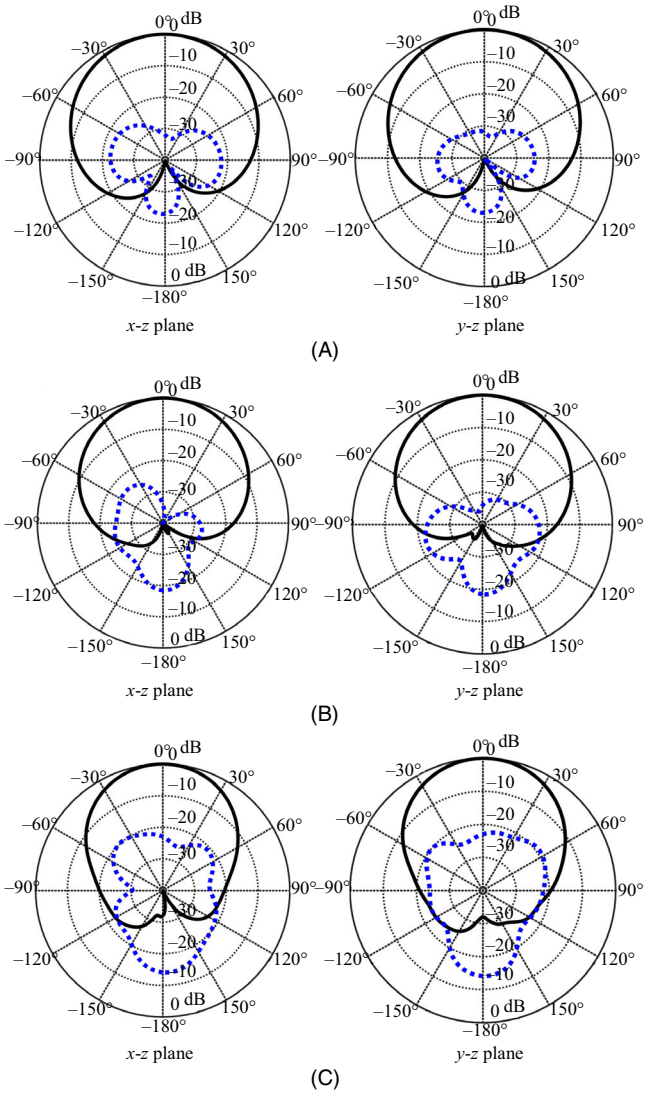

FIGURE 9 Normalized circularly polarized radiation patterns at (A) 3.5 GHz, (B) 4.5 GHz, and (C) 5.4 GHz (LHCP pattern: solid line; right-hand circularly polarized pattern: dotted line)

The AR and gain of the antenna obtained via the HFSS and CST simulations are shown in Figure 7, where it can be seen that there was good agreement between the two methods. The antenna had a peak gain of 9 dB and an average gain of 8.5 dB, which is about 3 dB better than that of a single patch without a stacked configuration. The AR bandwidth of the antenna was found to be 64% (2.82 GHz to 5.69 GHz), which covered the entire frequency range where the antenna was matched. The AR bandwidth of this antenna was about 18% higher than that of the antenna shown in Figure 1, and 14% higher than the antenna described in Mashhadi et al. [22]. Based on these results, the stacked multi-resonator structure increased both the impedance and AR bandwidths.

In Figure 8, the AR pattern of the antenna in the two planes of $\varphi = 0°$ and $\varphi = 90°$ is shown for different

frequencies. As shown in the figure, the antenna had a very wide AR beamwidth (more than 120°) if the frequency was not very high. However, the AR beamwidth was reduced at high frequencies due to the increased contribution of the counter clockwise mode. Nevertheless, a minimum AR beamwidth of 70° was obtained across the band of interest. Such a design is anticipated to be attractive in various applications requiring a wide-angle circular polarization, such as GPS.

The normalized LHCP radiation pattern of the antenna in the $\varphi = 0°$ and $\varphi = 90°$ planes at frequencies of 3.5 GHz, 4.5 GHz, and 5.4 GHz is shown in Figure 9. As shown, due to the symmetrical antenna configuration, the radiation patterns were symmetrical at the center frequency and two edged-band frequencies for both the *x*-*z* and *y*-*z* planes. Note that the forward to backward ratio decreased from 23 dB to 14 dB when the frequency increased from 3.5 GHz to 5.4 GHz.

The effect of the magnetic bias fields on the return loss, gain, and AR of the antenna is shown in Figure 10. As can be seen in Figure 10A, when the magnetic bias field H_0 was increased from 500 A/m to 35,000 A/m, the impedance bandwidth decreased slightly and the center frequency of the antenna shifted higher. This property can be exploited to accomplish small adjustments in the tuning of the center frequency of the antenna. The plot in Figure 10B shows that the ARs were maintained below 3 dB in the radiation frequency range of the antenna for all values of H_0 and the peak gain of the antenna remained at 9 dB by changing the magnetic bias field.

Until now, it was assumed that the ferrite was uniformly biased, although in practice there is some nonuniformity in the bias. Thus, to verify the previous results, in an experiment, an NdFeB rare-earth magnet (grade N45, $B_r = 1.35$ T, $BH_{max} = 45$ MGOe) with dimensions of 100 mm × 100 mm 8 mm was placed 5 mm below the ground plane to bias the ferrite substrate. In this case, the average magnetic bias field in the ferrite with the permanent magnet in position was approximately 15,000 A/m. In practice, permanent magnets are weak at the center and strong around the

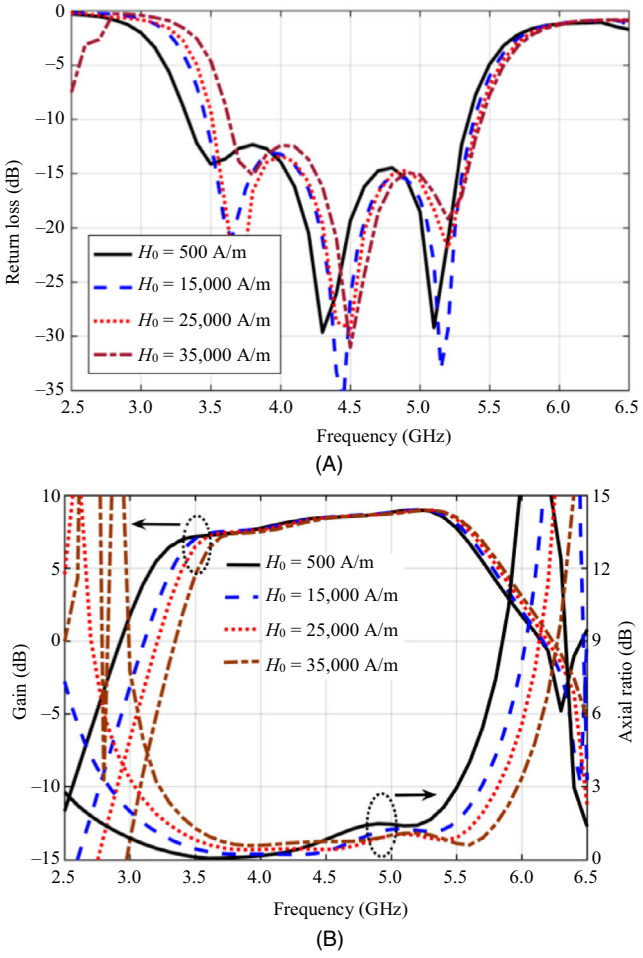

FIGURE 10 Effect of magnetic DC bias field H_0 on: (A) return loss, and (B) gain and AR of antenna shown in Figure 5

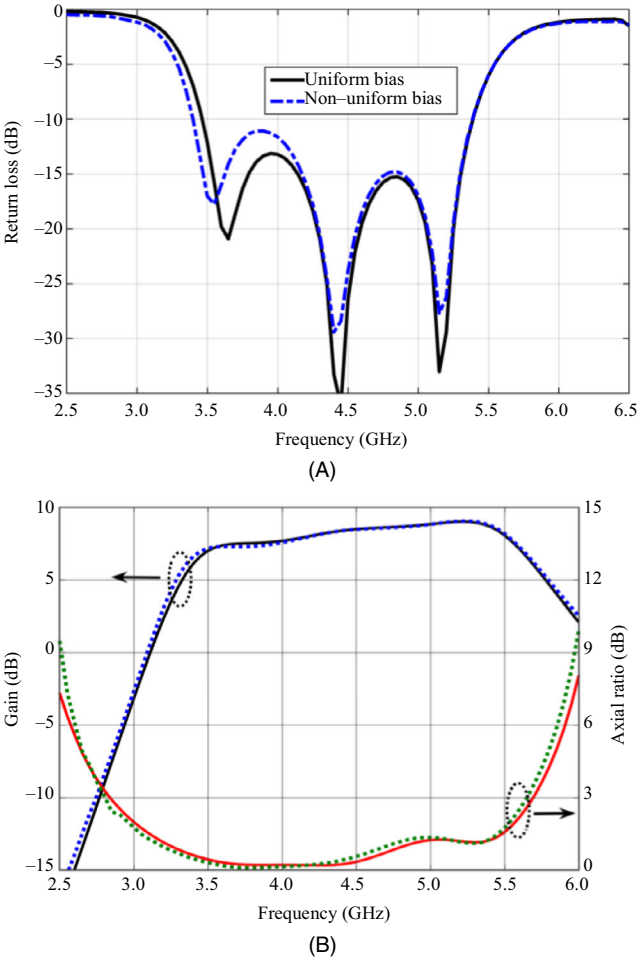

FIGURE 11 Comparison of (A) return loss, (B) gain, and AR of antenna when uniform and nonuniform bias fields were considered (solid line represents uniform bias; dotted line represents nonuniform bias)

TABLE 1 Comparison between proposed and other wideband CP antennas

Ref.	Center frequency (GHz)	Volume (λ_0^3)	S_{11} BW (%)	AR BW (%)	Peak gain (dB)
[6]	2.49	1.1 × 1.1 × 0.13	49.8	24	≅9
[7]	5.25	0.6 × 0.49 × 0.07	33.7	18.5	≅6
[8]	2.5	1.71 × 1.71 × 0.13	28.4	23.6	13
[9]	5.75	0.86 × 0.86 × 0.03	29	15.5	8.25
[10]	2.95	0.4 × 0.4 × 0.016	58	20	3.5
[12]	5.52	1.1 × 0.92 × 0.03	>130	44.3	5
[13]	2.42	0.69 × 0.57 × 0.01	57	39.4	3.4
[15]	2	0.75 × 0.75 × 0.01	60	62.5	1.7
[16]	6	1.75 × 1.75 × 0.42	~130	40	10
[17]	3.5	1.75 × 1.75 × 0.29	74.3	62	≅7.5
[22]	4.1	0.68 × 0.68 × 0.02	15.5	50	7.9
[34]	8.65	0.62 × 0.62 × 0.35	36.2	34	9
[35]	2.62	1.1 × 1.1 × 0.24	38.2	28.6	8.34
[36]	4	0.82 × 1.18 × 0.06	36	28.3	7.5
This work	4.42	0.74 × 0.74 × 0.1	44	64	9

edges. Therefore, the length of the permanent magnet was assumed to be larger than that of the ferrite so that the nonuniformity of the magnetic fields in the ferrite was smaller. The return loss of the antenna depicted in Figure 5 in both uniform and nonuniform bias situations is shown in Figure 11A, where it can be seen that there was good agreement between the return losses obtained from both biases. The AR and gain of the antenna obtained for uniform and nonuniform bias fields is shown in Figure 11B. As shown, there was good agreement between the two situations, which indicates that a uniform bias field is a good approximation and that the proposed antenna is eminently practical.

The performance of the proposed CP antenna is compared with that of other recent works in Table 1. As shown, the proposed antenna had a wider AR bandwidth than that of the antennas proposed in [6–10] and a narrower impedance bandwidth than the antennas in references [10,12,13,15], although the proposed antenna exhibited a higher peak gain. When compared to the antennas in references [16,17], the proposed antenna had a smaller impedance bandwidth, a comparable AR bandwidth and peak gain, and a significantly smaller size. In comparison with the antenna in Mashhadi et al. [22], the proposed antenna had a wider AR and impedance bandwidth and a higher peak gain. However, in this case, the proposed antenna was larger overall due to the stacked configuration. Finally, in comparison to the antennas described in references [34–36], the proposed antenna had a wider AR bandwidth, impedance bandwidth, and contiguous peak gain.

4 | CONCLUSIONS

The antenna proposed in this paper consisted of a circular patch antenna on a two-layer, ferrite-dielectric substrate with a wideband circular polarization. The first two resonance frequencies of the developed antenna were related to the clockwise and counter clockwise resonant modes and were far enough apart in the negative permeability range to produce a wide AR bandwidth. In addition, parasitic patches in a stacked configuration were employed to improve the impedance bandwidth. The simulation results show the proposed antenna had an impedance bandwidth of 44% and an AR bandwidth of 64%.

ORCID

Nader Komjani https://orcid.org/0000-0002-2420-9226

REFERENCES

1. Q. W. Lin et al., *Printed meandering probe-fed circularly polarized patch antenna with wide bandwidth*, IEEE Antennas Wireless Propag. Lett. **13** (2014) 654–657.
2. Nasimuddin, Z. N. Chen, and X. Qing, *A compact circularly polarized cross-shaped slotted microstrip antenna*, IEEE Trans. Antennas Propag. **60** (2012), no. 3, 1584–1588.
3. K. Wong and Y. Lin, *Circularly polarized microstrip antenna with a tuning stub*, Electron. Lett. **34** (1998) no. 9, 831–832.
4. Yohandri, J. T. S. Sumantyo, and H. Kuze, *A new triple proximity-fed circularly polarized microstrip antenna*, AEU-Int. J. Electron. Commun. **66** (2012), no. 5, 359–400.
5. N. R. Pasumarthy and P. R. Yagateela, *Compact single feed circularly polarized koch island microstrip antenna*, AEU-Int. J. Electron. Commun. **70** (2016), no. 11, 1543–1550.
6. J. Wu et al., *Broadband circularly polarized patch antenna with parasitic strips*, IEEE Antennas Wireless Propag. Lett. **14** (2015), 559–562.
7. Z. Wu et al., *Metasurface superstrate antenna with wideband circular polarization for satellite communication application*, IEEE Antennas Wireless Propag. Lett. **15** (2016), 374–377.
8. X. Jiang et al., *A low-cost wideband circularly polarized slot array with integrated feeding network and reduced height*, IEEE Antennas Wireless Propag. Lett. **15** (2016), 222–225.
9. S. Maddio, *A compact wideband circularly polarized antenna array for c-band applications*, IEEE Antennas Wireless Propag. Lett. **14** (2015), 1081–1084.
10. M. Rahimi et al., *Wide band srr-inspired slot antenna with circular polarization for wireless application*, AEU-Int. J. Electron. Commun. **70** (2016), no. 9, 1199–1204.
11. Q. Liu et al., *Compact wideband circularly polarized patch antenna for cnss applications*, IEEE Antennas Wireless Propag. Lett. **12** (2013), 1280–1283.

12. R. V. Krishna and R. Kumar, *Design of ultra wideband trapezoidal shape slot antenna with circular polarization*, AEU-Int. J. Electron. Commun. **67** (2013), no. 12, 1038–1047.
13. H. G. Xue, X. X. Yang, and Z. Ma, *A novel microstrip-CPW fed planar slot antenna with broadband and circular polarization*, IEEE Antennas Wireless Propag. Lett. **14** (2015), 1392–1395.
14. K. Jono and T. Fujimoto, *Wideband rectangular printed monopole antenna for circular polarisation*, IET Microwaves Antennas Propag. **8** (2014), no. 9, 649–656.
15. A. Panahi et al., *A printed triangular monopole with wideband circular polarization*, IEEE Trans. Antennas Propag. **63** (2015), no. 1, 415–418.
16. R. V. Krishna, R. Kumar, and N. Kushwaha, *A circularly polarized slot antenna for high gain applications*, AEU-Int. J. Electron. Commun. **68** (2014), no. 11, 1119–1128.
17. N. Kushwaha and R. Kumar, *Design of a wideband high gain antenna using FSS for circularly polarized applications*, AEU - Int. J. Electron. Commun. **70** (2016), no. 9, 1156–1163.
18. K. K. Tsang and R. J. Langley, *Design of circular patch antennas on ferrite substrates*, IEE Proc.-Microwaves Antennas Propag. **145** (1998), no. 1, 49–55.
19. D. Pozar, *Radiation and scattering characteristics of microstrip antennas on normally biased ferrite substrates*, IEEE Trans. Antennas Propag. **40** (1992), no. 9, 1084–1092.
20. A. A. Mavridis, G. A. Kyriacou, and J. N. Sahalos, *Analysis of circular patch antenna tuned by a ferrite post*, Microw. Opt. Technol. Lett. **46** (2005), no. 3, 234–237.
21. J. Ghalibafan, B. Rejaei, and N. Komjani, *A circularly polarized antenna based on the unidirectional resonant modes of a ferrite disk*, IEEE Trans. Magn. **50** (2014), no. 3, 88–95.
22. M. Mashhadi et al., *Analysis of wideband circularly polarized ferrite-loaded antenna based on unidirectional resonant modes*, IEEE Trans. Magn. **53** (2017), no. 9, 1–8.
23. S. Bedra, S. Benkouda, and T. Fortaki, *An efficient study of circular microstrip antenna on suspended and composite substrates*, J. Comput. Electron. **16** (2017), no. 3, 922–929.
24. P. Malathi and R. Kumar, *Design of multilayer rectangular microstrip antenna using artificial neural networks*, Int. J. Recent Trends Eng. **2** (2009), no. 5, 53–57.
25. Nasimuddin, K. Esselle, and A. K. Verma, *Fast and accurate model for circular microstrip antennas on suspended and composite substrates*, IEEE Trans. Antennas Propag. **53** (2005), no. 9, 3097–3100.
26. G. Kumar and K.P. Ray, *Broadband microstrip antennas*, Artech House, Boston, USA, 2003, pp. 89–200.
27. N. Liu, L. Zhu, and W. Choi, *A differential-fed microstrip patch antenna with bandwidth enhancement under operation of TM 10 and tm 30 modes*, IEEE Trans. Antennas Propag. **65** (2017), no. 4, 607–1614.
28. N. Liu, L. Zhu, and W. Choi, *A low-profile wide-bandwidth planar inverted-F antenna under dual resonances: Principle and design approach*, IEEE Trans. Antennas Propag. **65** (2017), no. 10, 5019–5025.
29. N. Liu et al., *A low-profile aperture-coupled microstrip antenna with enhanced bandwidth under dual resonance*, IEEE Trans. Antennas Propag. **65** (2017), no. 3, 1055–1062.
30. N. Liu et al., *Wideband shorted patch antenna under radiation of dual-resonant modes*, IEEE Trans. Antennas Propag. **65** (2017), no. 6, 2789–2796.
31. A. Boutejdar, A. A. Ibrahim, and E. P. Burte, *A compact multiple band-notched planer antenna with enhanced bandwidth using parasitic strip lumped capacitors and DGS-technique, Telkomnika Indones*. J. Electr. Eng. **13** (2015), no. 2, 203–208.
32. A. Boutejdar et al., *Design and fabrication of a novel quadruple- band monopole antenna using a U-DGS and open- loop-ring resonators*, Advanced Electromagn. **6** (2017), no. 3, 59–63.
33. S. Fu et al., *Broadband circularly polarized microstrip antenna with coplanar parasitic ring slot patch for L-band satellite system application*, IEEE Antennas Wireless Propag. Lett. **13** (2014), no. 9, 943–946.
34. H. Oraizi and R. Pazoki, *Wideband circularly polarized aperture-fed rotated stacked patch antenna*, IEEE Trans. Antennas Propag. **61** (2013), no. 3, 1048–1054.
35. J. Baik et al., *Broadband circularly polarized crossed dipole with parasitic loop resonators and its arrays*, IEEE Trans. Antennas Propag. **59** (2011), no. 1, 80–88.
36. N. Nasimuddin, Z. N. Chen, and X. Qing, *Bandwidth enhancement of a single-feed circularly polarized antenna using a metasurface: metamaterial-based wideband CP rectangular microstrip antenna*, IEEE Antennas Propag. Mag. **58** (2016), no. 2, 39–46.

AUTHOR BIOGRAPHIES

Mostafa Mashhadi received a BSc degree in electrical engineering from Ferdowsi University, Mashhad, Iran, in 2008 and an MSc degree in communications engineering from the Iran University of Science and Technology, Tehran in 2011, where he is currently working toward a PhD degree. His research interests include microstrip antennas, passive magnetic devices, and scattering.

Nader Komjani received BS, MS, and PhD degrees in electrical engineering from the Iran University of Science and Technology (IUST), Tehran, Iran, in 1988, 1991, and 2000, respectively. He is currently an associate professor and the head of the millimeter-wave laboratory in IUST. He has authored or co-authored more than 90 papers in journals and conferences. His research interests include the areas of ultrawide band and multiband microstrip antennas, numerical methods in electromagnetics, reflected array and phased array antennas, and passive and active microwave and millimeter-wave systems.

Behzad Rejaei received an MSc degree in electrical engineering from the Delft University of Technology, Delft, the Netherlands, in 1990, and a PhD degree in theoretical condensed matter physics from the University of Leiden, Leiden, the Netherlands, in 1994. From 1995 to 1997, he served as a member of the Physics Faculty at the Delft University of Technology, where he conducted research on mesoscopic charge-density-wave systems. Between 1997 and 2010, he was with the Department of Electrical Engineering, Mathematics, and Computer Science at the Delft University of Technology. He is currently an associate professor in the Department of Electrical Engineering, Sharif University of Technology, Tehran, Iran. His research interests are in the areas of the electromagnetic modeling of integrated passive components, passive magnetic devices, and graphene plasmonics.

Javad Ghalibafan received a BS degree from the Ferdowsi University of Mashhad in 2007 and MS and PhD degrees from the Iran University of Science Technology in 2009 and 2013, respectively. In 2014, he joined the Department of Electrical Engineering, Shahrood University of Technology, Shahrood, Iran, where he is now assistant professor and the head of the Antenna & Microwave Lab. His research interests include the analysis, design, and measurement of artificial electromagnetic materials; antenna and microwave devices; metamaterials; and magnetic materials.